Shifts in water supply and demand drive land cover change across Chile[1]

Francisco Zambrano[a,b], Anton Vrieling[c], Francisco Meza[d,e,f], Iongel Duran-Llacer[g], Francisco Fernández[b,h,i], Alejandro Venegas-González[b,j], Nicolas Raab[d], and Dylan Craven[b,k,l]

[a] Hémera Centro de Observación de la Tierra, Facultad de Ciencias, Escuela de Ingeniería en Medio Ambiente y Sustentabilidad, Universidad Mayor, Santiago,, Chile.

[b] Observatorio de Sequía para la Agricultura y la Biodiversidad de Chile (ODES), Universidad Mayor, Santiago, Chile.

[c] Faculty of Geo-Information Science and Earth Observation (ITC), University of Twente, Enschede, The Netherlands.

[d] Facultad de Agronomía y Sistemas Naturales, Pontificia Universidad Católica de Chile., Santiago, Chile.

[e] Instituto para el Desarrollo Sustentable. Pontificia Universidad Católica de Chile, Santiago, Chile.

[f] Centro Interdisciplinario de Cambio Global, Pontificia Universidad Católica de Chile, Santiago, Chile.

[g] Hémera Centro de Observación de la Tierra, Facultad de Ciencias, Universidad Mayor, Santiago, Chile.

[h] Center of Economics for Sustainable Development (CEDES), Faculty of Economics and Government, Universidad San Sebastián, Santiago, Chile.

[i] Center of Applied Ecology and Sustainability (CAPES), Santiago, Chile.

[j] Instituto de Ciencias Agroalimentarias, Animales y Ambientales (ICA3), Universidad de O'Higgins, San Fernando, Chile.

[k] GEMA Center for Genomics, Ecology & Environment, Universidad Mayor, Camino La Pirámide Huechuraba 5750, Santiago, Chile.

[l] Data Observatory Foundation, Santiago, Chile.

Corresponding author. Email: francisco.zambrano@umayor.cl

Abstract

Globally, droughts are becoming longer, more frequent and more severe, and their impacts are multidimensional. These impacts typically extend beyond the water balance as long-term, cumulative changes in the water balance can lead to regime shifts in land use. Here, we assess the effects of temporal changes in water supply and demand on vegetation productivity and land cover change over multiple time scales in continental Chile, which has experienced a severe drought over the last 20 years. Across most of continental Chile, we found a persistent decreasing trend in water supply and an increasing trend in water demand since 1981, trends that intensify over longer time scales. This long-term decrease in water availability has led to a decrease in vegetation productivity, especially in central and southern Chile. Our models suggest that increasing drought severity has led to shifts in land use towards more drought-tolerant land cover types, such as shrublands. We also found evidence that human perceptions of prolonged drought can indirectly lead to large-scale changes in land use. Our results suggest that long-term climate change may lead to regime shifts in land cover that can be mitigated by context-specific adaptation strategies.

[1] This paper is a non-peer reviewed preprint submitted to EarthArXiv.

Introduction

Across many regions of the world, droughts are becoming longer, more frequent, and more severe[1,2], impacting ecosystems *via* tree mortality[3] and productivity[1] and inducing shifts in land use and cover[4]. However, identifying drought events is idiosyncratic due to the varying criteria used for classification. Droughts can be classified as either 1) meteorological, i.e., when precipitation in a specific period falls below mean precipitation values observed over multiple years (usually more than 30 years); 2) hydrological, i.e., when precipitation anomalies last for long periods (months to years) and affect water systems; 3) agricultural, i.e. when precipitation deficits negatively impact plant health, leading to decreases in crop or pasture productivity[5]; or 4) ecological, i.e., when precipitation deficits negatively affect the provisioning of ecosystem services and trigger feedbacks in natural or human systems[4]. Such feedbacks include drought impacts on human decision making and activities, which can lead to land-use change[6,7], which may have cascading effects on biodiversity and ecosystem services (e.g., ref. 8, 9).

Despite the high degree of confidence in the impacts of rising temperatures on the extent, frequency, and severity of agricultural and ecological droughts[2], which are likely to increase even if global warming stabilizes at 1.5°–2°C, the severity of meteorological droughts has been remarkably stable globally over the past century[10,11]. In the few regions where drought severity has increased over this period (1900-2000), rising temperatures have increased atmospheric evaporative demand (AED), which has been associated with increases in agricultural land area[10]. Thus, rising water demand may reflect parallel changes in land use - primarily agriculture - that can exacerbate the effects of meteorological droughts on ecosystems.

From 1960 to 2019, land-use change has impacted approximately one-third of the Earth's surface, which is four times more than previously thought[12]. Despite the considerable interest in land-use change dynamics (e.g. ref. 12, 13), the direction and magnitude of drought impacts on land cover change and vegetation productivity remain uncertain[14-16]. While meteorological droughts are responsible for approximately 37% of land cover change and variability in vegetation productivity globally[16], there is little support for the idea that meteorological droughts affect soil moisture[14]. However, the evidence supporting these results is derived from only one drought index, Standardized Precipitation Evapotranspiration Index (SPEI; ref. 17), which combines a proxy for water supply - precipitation - with a proxy for water demand - AED - at one time scale (12 months). The use of only one time scale may bias results of drought impacts towards ecosystems dominated by plant growth forms such as grasses and herbs that respond more rapidly to drought stress (< 12 months). This is because physiological differences among and within dominant plant growth forms may increase (or decrease) tolerance of drought stress[18,19]. For example, trees growing in more arid ecosystems typically respond over longer time scales than those in more humid ecosystems[20].

Expanding analyses to include multiple dimensions of droughts can provide complementary insights into the Earth's water balance - and its impacts - over multiple time scales. Yet, the World Meteorological Organization recommends the use of a single drought index for monitoring droughts[21], i.e., the multi-scale Standardized Precipitation

Index (SPI; ref. 22), but is limited in that it only looks at water supply in the form of precipitation. The SPEI builds upon SPI by incorporating the effects of temperature on droughts, and is now used widely for drought monitoring (e.g., ref. 23, 24). To better disentangle the effects of precipitation from those of temperature[25], as well as to capture droughts in terms of water demand, AED has been integrated into the Evaporative Demand Drought Index (EDDI; ref. 26), which is particularly effective at detecting the rapid onset or intensification of droughts. Indices derived from soil moisture products, such as the Soil Moisture Deficit Index (SDMI; ref. 27), the Soil Moisture Agricultural Drought Index (SMADI; ref. 28), and the Standardized Soil Moisture Index (SSI; ref. 29, 30) also monitor water supply and are thought to better capture water availability for crops, thus providing more relevant information for evaluating agricultural droughts. In turn, ecological droughts, which capture the joint impacts of precipitation and temperature on natural and productive ecosystems *via* variation in net primary productivity[31-33], are usually monitored with the Normalized Difference Vegetation Index (NDVI) and derived anomaly indices, e.g., zcNDVI[34]. However, none of the aforementioned drought indices directly or indirectly consider the broader impacts of droughts on human decisions and activities - particularly land-use change, which is critical to developing a more holistic view of climate change impacts.

Here, we analyze the multi-dimensional impacts of drought on water supply and demand, net primary productivity, and land-use change across terrestrial ecosystems in continental Chile. Chile's diverse climate and ecosystems[35,36] make it an ideal natural laboratory for assessing the dynamic interactions between climate and ecosystems, and potential impacts on land-use change. Additionally, large parts of Chile have experienced severe drought conditions that have significantly affected vegetation and water storage in recent years; north-central Chile has faced a persistent precipitation deficit (or "mega-drought") since 2010[37], which has broadly impacted native forests (e.g., ref. 38-40) and agricultural productivity (e.g., ref. 34, 41, 42). There is also growing evidence that this "mega-drought" has impacted farmers' decision making, shifting to crop systems with shorter rotations and lower capital costs[43]. Given the persistent water deficit associated with the "mega-drought" and its cascading effects on the hydrological system[44], it is critical to assess multiple time scales that account for the cumulative impacts of this extreme event over several years. We therefore aim to assess: i) short- to long-term time trends in multi-scalar drought indices that capture variation in the components of water balance, i.e., water supply and demand; ii) temporal changes in land-use cover and vegetation productivity, and iii) drought impacts on vegetation productivity and land-use change across continental Chile.

Results

Decreases in water supply and increases in water demand strengthen over longer time scales

We observed a temporal decrease in SPI, SPEI, and SSI - proxies largely associated with water supply - from north to south in continental Chile, with the exception of the southernmost region ("Austral"), a trend that became more pronounced when considering longer time scales (Fig. 1). In contrast, we found that EDDI - a proxy for atmospheric water demand - showed a positive trend across Chile, with a sharper increase over time scales in

the north than in the south. In general, these results suggest that declines in precipitation have reduced water supply, while increases in temperature have increased water demand over the past four decades.

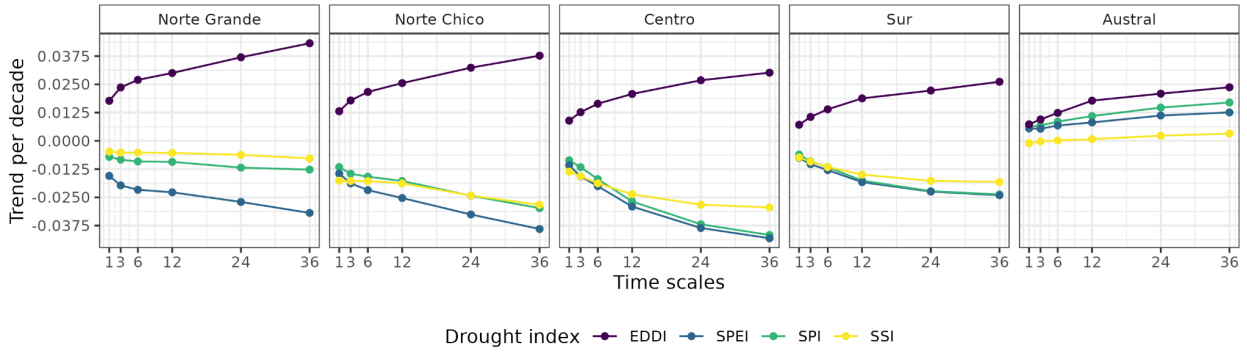

Figure 1. Drought severity increases over longer time scales across most of continental Chile. Temporal shifts in drought severity over multiple time scales for indices associated with water supply (SPI, SPEI, SSI) and demand (EDDI) across continental Chile for 1981-2023. SPI is the standardized precipitation index, SPEI is the Standardized Precipitation Evapotranspiration Index , SSI is the Standardized Soil Moisture Index, and EDDI is the Evaporative Demand Drought Index. Drought indices were aggregated per region for visualization.

Vegetation productivity decreased in northern and central Chile

Despite evidence of increasing drought severity across Chile, we found contrasting temporal trends in vegetation productivity (Fig. 2). In the two southernmost regions ('Sur' and 'Austral') and one northern region ('Norte Grande'), vegetation productivity increased over the last 23 years, while in two more central regions ('Centro' and 'Norte Chico') it decreased over the same period (Fig. 2). In central Chile, vegetation productivity was lowest from 2019 to 2022, which could be due to either a decrease in vegetation area, a loss of biomass or browning in forest ecosystems.

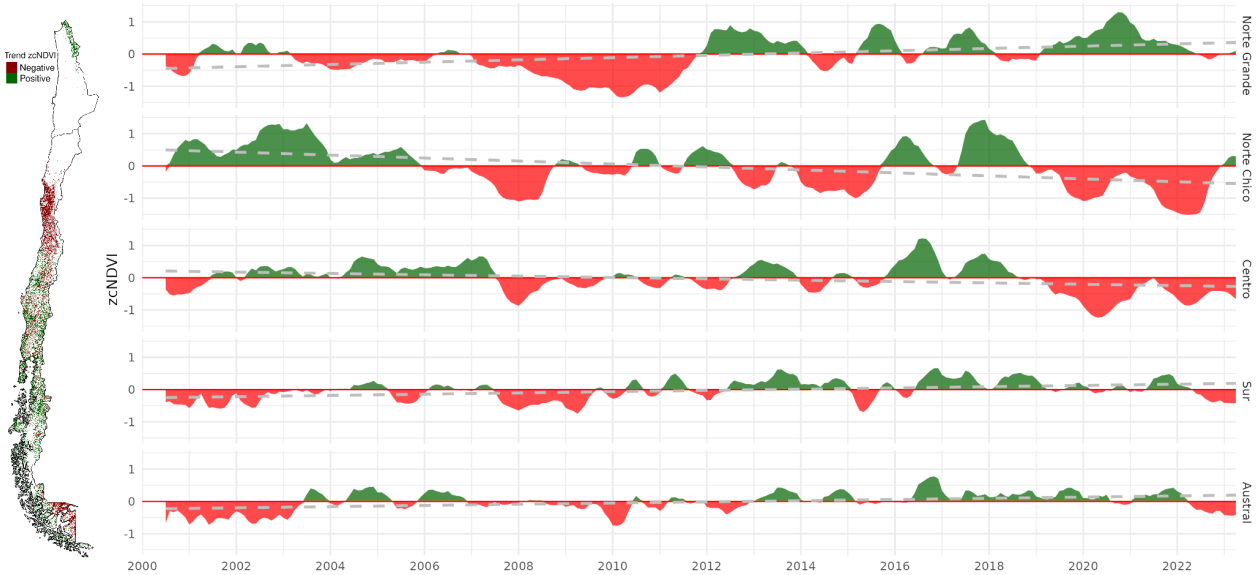

Figure 2. Central and northern Chile have experienced the greatest decline in vegetation productivity. Spatial (**a**) and temporal (**b**) variation in vegetation productivity across continental Chile for 2000-2023. Vegetation productivity was estimated as standardized vegetation productivity (zcNDVI). Green corresponds to areas with a positive temporal trend in zcNDVI, red corresponds to a negative temporal trend in zcNDVI, and gray corresponds to areas that did not change over time. Temporal trends in zcNDVI were estimated with the non-parametric modified Mann-Kendall test for serially correlated data.

Cropland and forest cover are shifting southwards

We also observed significant changes in land cover across continental Chile (Fig. 3). In northern Chile ("Norte Grande" and "Norte Chico"), the area of croplands (-12 km^2yr^{-1}) and savannas (-70 km^2yr^{-1}) decreased, while that of barren lands increased significantly (111 km^2yr^{-1}) and the area of forests, grasslands and shrublands did not change (0 km^2yr^{-1}). In central Chile ("Centro"), croplands (-22 km^2yr^{-1}) and savannas (-136 km^2yr^{-1}) experienced a strong decline in area, but the area of shrublands (146 km^2yr^{-1}), grasslands (83 km^2yr^{-1}), and barren lands (23 km^2yr^{-1}) increased, and the area of forests did not change (0 km^2yr^{-1}). In contrast, in southern Chile ("Sur"), forest (397 km^2yr^{-1}) and cropland (38 km^2yr^{-1}) area increased over time, with only the area of savannas decreasing (-319 km^2yr^{-1}). In the southernmost region ("Austral"), only the area of savannas increased (172 km^2yr^{-1}), while the area of barren land (-93 km^2yr^{-1}) and shrublands (-37 km^2yr^{-1}) decreased. These results suggest that croplands are shifting further south, from northern and central Chile to southern Chile, where savannas are being rapidly replaced by native and planted forests.

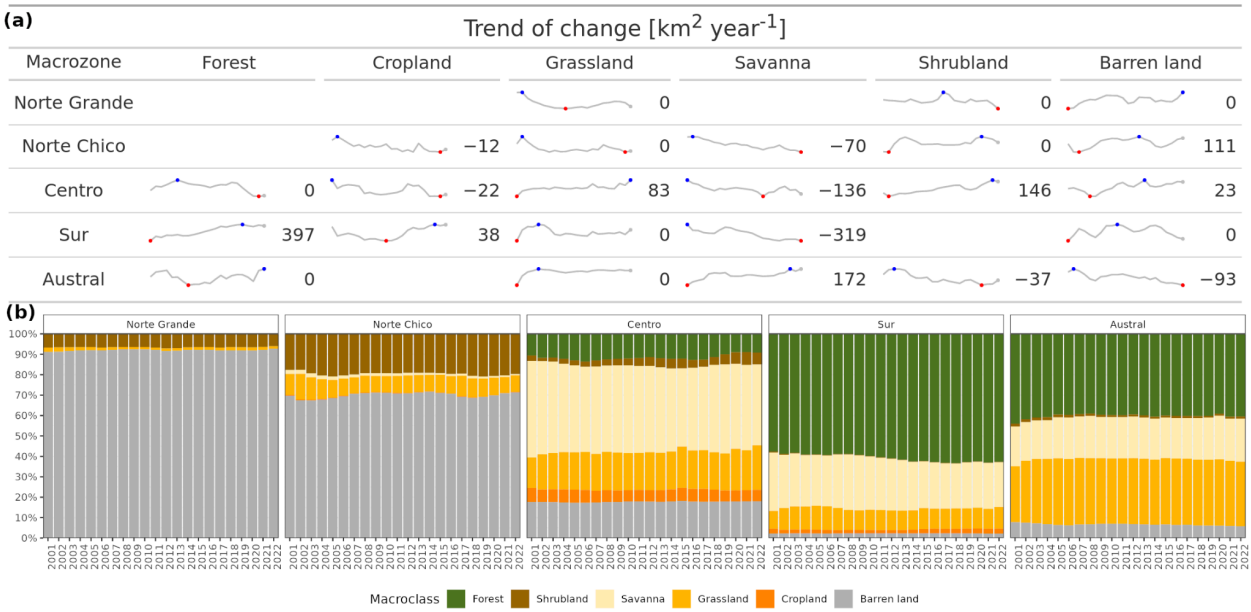

Figure 3. **Land cover is shifting dynamically across continental Chile**. Temporal trends in absolute (**a**) and relative (**b**) land cover across continental Chile for 2001-2022. Temporal change in area for each class was estimated with Sen's slope; zero values indicate no change, while red and blue points indicate maximum and minimum values, respectively. Land cover classes with no values did not have statistically significant changes in area over the study period. Relative land cover change was estimated within each study region.

Drought impact on vegetation productivity are strongest in south-central Chile

We found that temporal variation in vegetation productivity was usually best explained by drought indices with time scales greater than 12 months (Fig. 4). For all drought indices, the time scales with the strongest correlation with vegetation productivity were longer towards northern Chile and shorter towards southern Chile, with the exception of the southernmost region ("Austral"). Especially in south-central Chile ("Centro" and "Sur"), the time scales with the strongest correlation with vegetation productivity were concentrated in the Coastal and Andean mountain ranges. However, the areas where vegetation was most affected by drought, i.e. where correlations were positive for SPI, SPEI and SSI and negative for EDDI, were located in south-central Chile, but not necessarily in either of the two mountain ranges. While the spatial variation in the relationship between drought intensity and vegetation productivity was consistent across drought indices, the drought index that captures water supply *via* soil moisture (Standardized Soil Moisture Index; SSI) tended to show a stronger correlation with vegetation productivity over larger areas than the other drought indices.

Our analysis also revealed that water demand and supply differentially affected the time scales at which vegetation productivity of land cover types within each region was most impacted by drought (Fig. 5/Table S1). In northern Chile, all land cover types exhibited stronger correlations with drought indices associated with water supply, i.e. SPI, SPEI, and SSI, at shorter time scales (12 or 14 months) than those associated with water demand, AED (36 months). In central Chile, we observed a similar pattern for shrublands and savannas, and found that vegetation productivity of shrublands, savannas, and croplands was generally more affected by changes in water supply than grasslands, croplands, or forests. In southern Chile, vegetation productivity within land cover types was less affected by variation in water supply or demand, and at shorter timescales than in other regions. Notably, vegetation productivity of native and planted forests was weakly correlated with drought indices ($-0.1 < r < 0.2$) at relatively long time scales, particularly in central Chile.

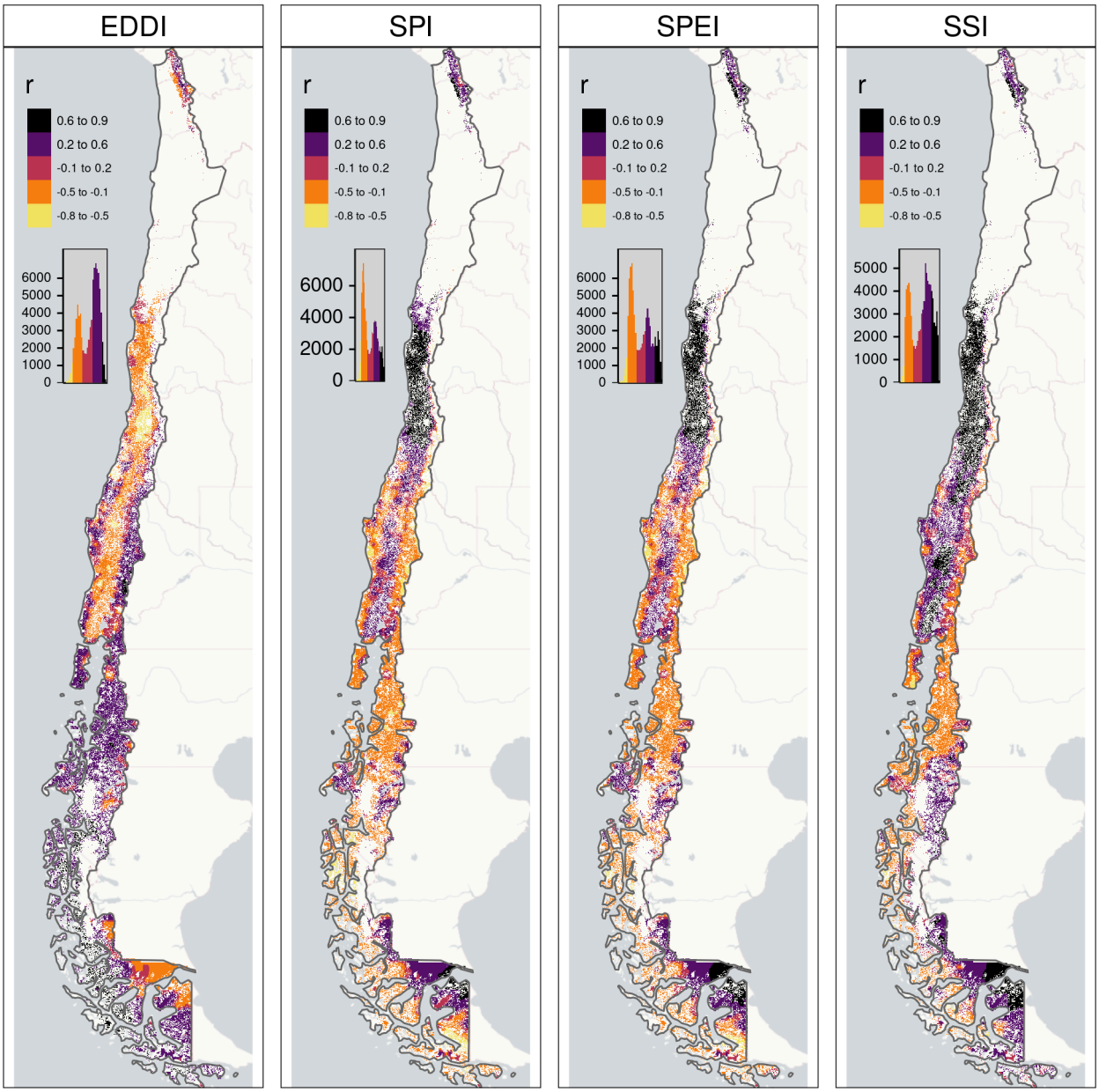

Figure 4. Drought impacts on vegetation productivity shift across continental Chile. Pearson's correlation coefficient was used to estimate the direction and magnitude of the relationship between drought severity and vegetation productivity for each index for 2000-2023. We show Pearson correlation coefficients for the time scale (3 - 36 months) at which they reach their maximum absolute value. In Chile, areas in white indicate no statistically significant correlation (p-value>0.05). SPI is the standardized precipitation index, SPEI is the Standardized Precipitation Evapotranspiration Index , SSI is the Standardized Soil Moisture Index, and EDDI is the Evaporative Demand Drought Index.

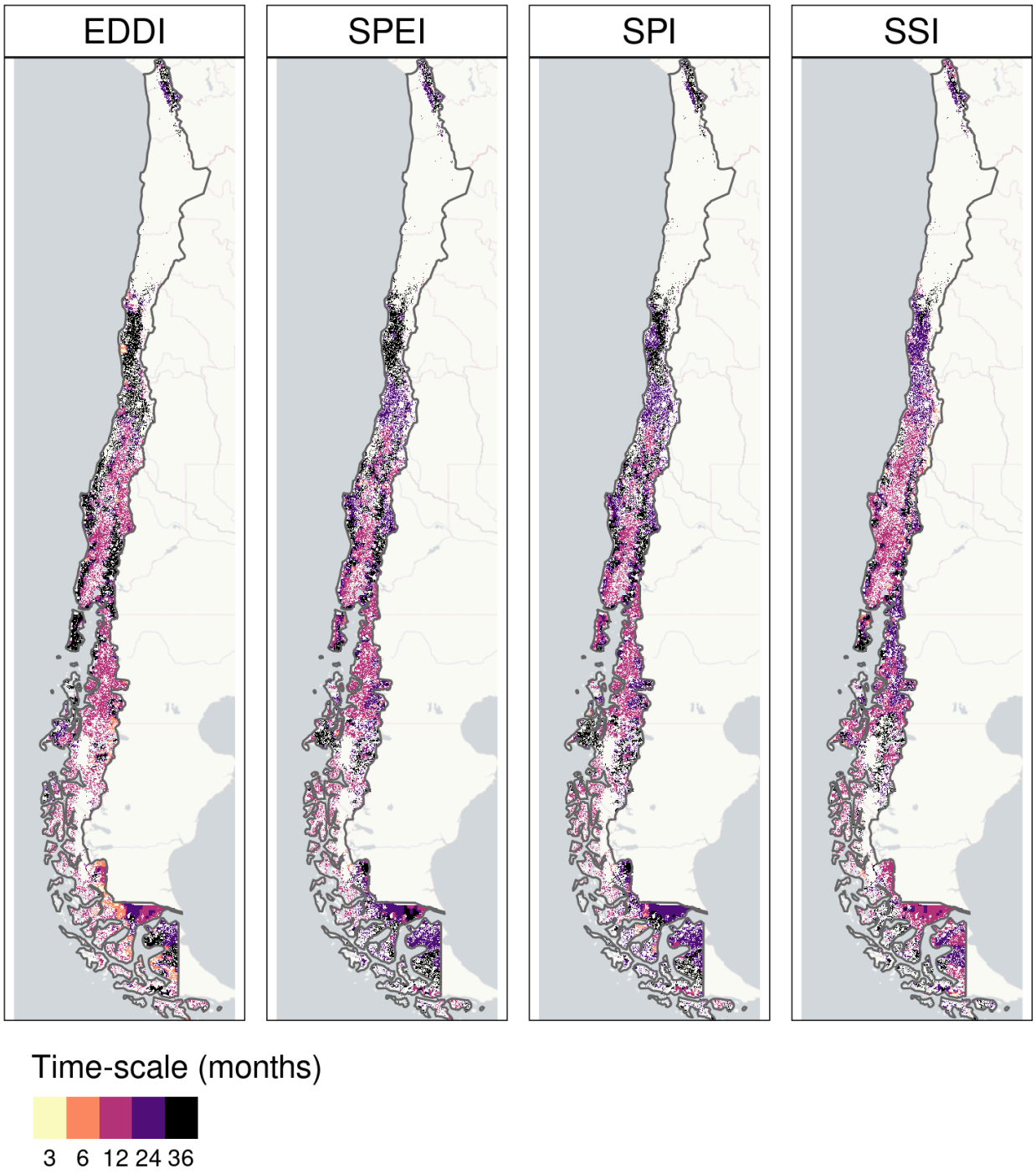

Figure 5. Drought impacts on vegetation productivity are higher over longer time scales. Spatial variation in the time scale (3-36 months) at which drought impacts on vegetation productivity are most severe across continental Chile for 2000-2023. In Chile, areas in white indicate no statistically significant correlation between vegetation productivity and drought severity (p-value>0.05). SPI is the standardized precipitation index, SPEI is the Standardized Precipitation Evapotranspiration Index , SSI is the Standardized Soil Moisture Index, and EDDI is the Evaporative Demand Drought Index.

Drought transforms land cover distribution

Our random forest models show that drought indices explain between 22-48% of the variation in land cover change across continental Chile, with the exception of croplands whose variation was weakly affected by drought (Fig. 6; 11-20%). Moreover, these results highlight the importance of considering water supply and demand, as drought indices associated with both aspects of the water balance had high importance values across most study regions and land cover types. The variation in the time scale of drought indices that provide the strongest correlation with vegetation productivity also suggests that different types of vegetation are not equally sensitive to droughts of similar intensities. For example, changes in savanna and shrubland cover were associated with longer time scales in most regions, while changes in forest cover in central and southern Chile were associated with shorter time scales. Our results also show that drought severity was associated with the magnitude and direction of land cover change (Fig. 7). More specifically, we found that decreases in precipitation (SPI-6) and soil moisture (SSI-36) and increases in atmospheric evaporative demand (EDDI-6 and EDDI-36) at multiple time scales are associated with non-linear decreases in grassland cover across continental Chile and forest cover from central to southern Chile. In contrast, shrubland cover increased non-linearly in response to decreases in precipitation (SPI-6 and SPI-36) and soil moisture (SSI-6 and SSI–36) and increases in atmospheric evaporative demand (EDDI-6 and EDDI-36) across central and northern Chile. Savanna cover responded weakly to changes in precipitation across continental Chile, but exhibited more pronounced non-linear declines in response to increasing atmospheric evaporative demand (EDDI-6 and EDDI-36) across most study regions. Cropland cover varied weakly in response to changes in either water supply or demand, likely due to the widespread use of irrigation and other practices that mitigate the effects of drought.

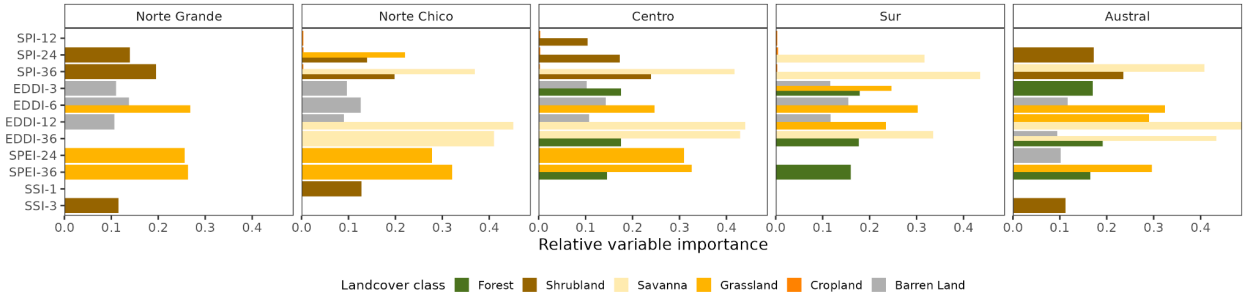

Figure 6. Shifts in water supply and demand drive land cover change across multiple time scales. Variable importance of multi-scalar drought indices for explaining land cover change in five study regions across continental Chile. Variable importance was estimated with Random Forest models fitted for each combination of study region and land cover type. SPI is the Standardized Precipitation *i*ndex, SPEI is the Standardized Precipitation Evapotranspiration Index , SSI is the Standardized Soil Moisture Index, and EDDI is the Evaporative Demand Drought Index. The numbers next to the drought index correspond to the time scales in months (1- 36).

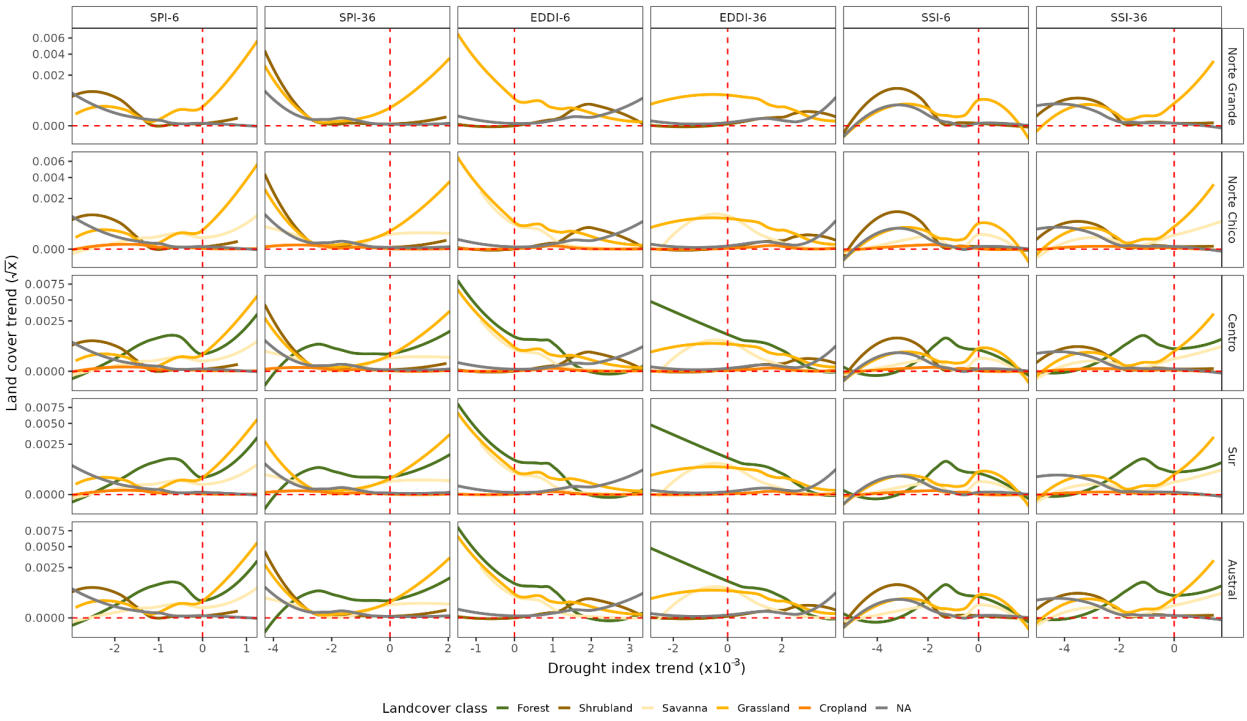

Figure 7. Drought severity drives land cover change, but not for all cover types. Response of land cover change in response to water demand and supply across multiple time scales and study regions in continental Chile. SPI is the Standardized Precipitation Index, SSI is the Standardized Soil Moisture Index, and EDDI is the Evaporative Demand Drought Index. For SPI and SSI, negative values are associated with more severe drought, while positive values of EDDI are associated with more severe drought. Numbers next to the drought index correspond to the time scales in months (1- 36). Fitted lines are smoothed response curves across river basins in each region estimated with Random Forest models. Results for other time scales and drought indices are provided in Supplementary Information (Figs. S2-S5).

Discussion

Temporal trends in water supply and demand

With the exception of the southernmost region, we found a significant decreasing trend in water supply (SPI, SPEI, and SSI) over the past four decades across continental Chile and is strongest in northern and central Chile[44,45]. Our results reveal that decreases in water supply increased over longer time scales, which is consistent with a progressive intensification of drought severity across much of Chile, as has been observed in other regions experiencing long-term droughts[46,47]. In parallel, we observed an increased water demand (EDDI) due to rising air temperatures, which also strengthened over longer time scales. Taken together, our results provide multiple lines of evidence that continental Chile has experienced a sustained drying trend due to a concurrent decrease in precipitation and increase in atmospheric evaporative demand[48].

Temporal trends in vegetation productivity

The consequences of the persistent drying trend for ecosystems throughout continental Chile are manifold. First, the prolonged hydrological drought, i.e. precipitation deficit, has reduced groundwater storage (SSI; ref. 49), leading to a steady decline in vegetation productivity (zcNDVI) since 2000 across northern and central Chile, reaching its lowest level between 2020 and 2022. This decline was most strongly associated with declines in soil moisture, as has been reported for natural and productive ecosystems[50-52]. Second, the strong coupling between vegetation productivity and soil moisture over longer time scales[53] that we observed provides a more direct physiological explanation for the sharp decline in forest growth and productivity in central Chile (e.g., ref. 1, 54), as the dominant woody vegetation (e.g., trees, shrubs) in this region is likely to obtain water from deeper in the soil profile than herbs, grasses, or agricultural crops[55]. Moreover, the strengthening of the correlation between vegetation productivity and water supply (SPI, SPEI, SSI) or demand (EDDI) over multiple time scales (up to 36 months) and across land cover types (Fig. 5) - demonstrates the impacts of climate change on the water balance in Chile. Impacts may extend beyond vegetation productivity, as reduced soil moisture in central Chile and the western United States has increased wildfire activity[56,57], which is a growing concern in Chile and may be further exacerbated by extensive plantations of highly flammable tree species, e.g., *Eucalyptus* spp. and *Pinus* spp.[58]. Third, we found that the decline in the vegetation productivity of croplands is due to a decrease in the water supply to a greater extent than to an increase in water demand[59], despite evidence that more water-intensive crops have replaced less water-intensive crops in central Chile, leading to an increase in water extraction from rivers or groundwater[60,61].

Drought impacts on land cover

We found evidence that temporal decreases in water supply and decreases in water demand are driving shifts not only in vegetation productivity but also in land cover across most of continental Chile. Forest and grassland cover were particularly sensitive to changes in the water balance over short and long temporal scales, which is consistent with recent studies showing that progressive, long-term water deficits in central Chile have triggered forest browning and declines in native forest productivity[1,38,54]. While our analysis do not distinguish between native and planted forests, the latter of which are considered to be more drought tolerant in central and southern Chile[62], we show that forest area declines more sharply in response to increasing water demand due to rising temperatures (EDDI) than decreasing water supply (e.g., SPI, SSI; refs. 63, 64), which may have cascading impacts on multiple facets of forest diversity[65,66]. Our results extend the results of these studies by showing that drought-induced forest cover decline has extended beyond central Chile to the southernmost region of continental Chile. This is noteworthy because declines in vegetation productivity in southern Chile - a region whose water balance is typically projected to be less affected by climate change than central and northern Chile[67] - have only manifested since 2022 (Fig. 2). Moreover, our results provide evidence that, in addition to forest cover, other land cover types have been affected by water deficits, particularly grasslands, despite physiological differences between dominant plant growth forms (e.g., trees, shrubs, C3 and C4 grasses; refs. 18, 19). Our results therefore suggest that multiple land cover types could

be vulnerable to regime shifts towards more drought tolerant land cover types[68,69], such as shrublands, whose cover increased non-linearly in response to increasing drought severity. In central Chile, for example, the increase in shrubland cover could be due to drought-induced decreases in savanna or cropland cover. Changes in cropland cover may not be a direct consequence of drought (Fig. 7), but rather an indirect one, possibly reflecting the decision of resource-poor farmers to migrate to regions with more abundant water resources or to change economic activity[7,70]. In contrast, the increase in shrubland cover due to a decrease in savanna cover may be ecological, as shrubs may be more drought tolerant than other growth forms[71,72].

Overall, our results show that long-term declines in water supply and demand have induced widespread, multi-dimensional impacts on the vegetation productivity and on the extent of land cover types. While prolonged droughts may directly cause shifts to more drought-tolerant land cover types, such as shrublands, they may also influence land cover change through human decision making and activities. This study extends current understanding of drought impacts by demonstrating how their multidimensionality emerges over multiple time scales and across land cover types, which can contribute to developing context-specific adaptation strategies for agriculture, biodiversity conservation, and natural resource management.

Materials and Methods

Study area

Continental Chile has a diverse climate, with strong gradients from north to south and east to west[73] (Fig. 8a), which, together with its complex topography, determine its ecosystem diversity[36,74] (Fig. 8c). We divided Chile into five regions: “Norte Grande” (17°34’–25°42’S), “Norte Chico” (25°42’-32°8’S), “Centro” (32°08’-36°12’S), “Sur” (36°12’-43°48’S), and “Austral” (43°48’-56°00’S). “Norte Grande” and “Norte Chico” are predominantly arid with hot (Bwh in the Koppen-Geiger classification) and cold (Bwk) temperatures. Towards the south of “Norte Chico”, the climate changes to an arid steppe with cold temperatures (Bsk). In these two northern regions, the land is mostly bare, with a small area covered by shrublands and grasslands. In the “Centro” region and the northern half of “Sur”, the climate is mostly Mediterranean, with warm to hot summers (Csa and Csb). Land cover in the “Centro” region consists of a significant amount of shrublands and savannas (50%), followed by grasslands (16%), forests (8%), and croplands (5%). The south of “Sur” and the north of the “Austral” region have a mostly oceanic climate (Cfb). Those zones have a large area of forests and grasslands. The southern part of the country has a tundra climate, while "Austral" is a cold, semi-arid area covered by grasslands and forests, and, to a lesser extent, savannas.

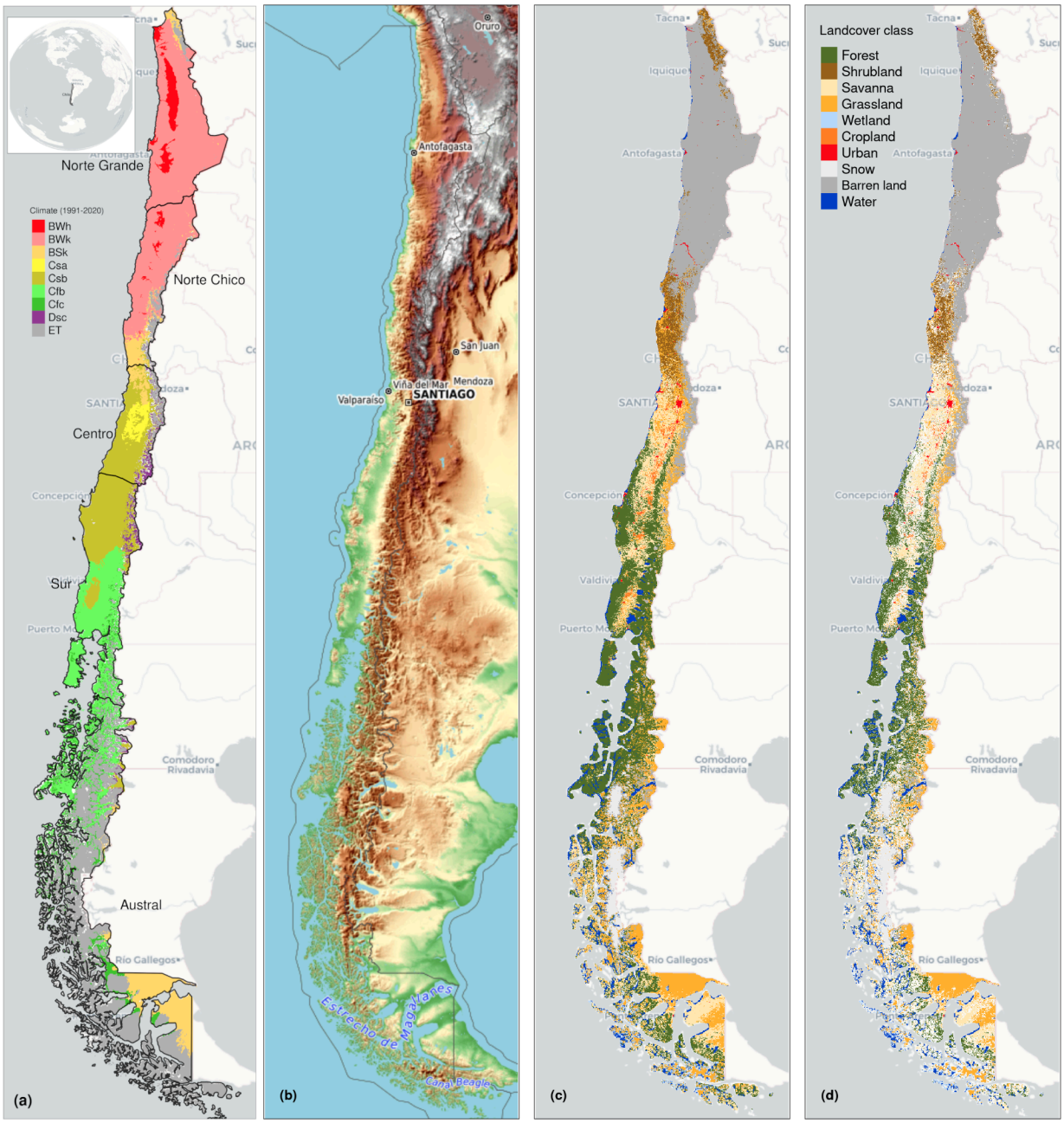

Figure 8. Climate, topography, and land cover classes across continental Chile. Koppen-Geiger climate classes (**a**), topography (**b**), land cover classes for 2022 (**c**), and persistent land cover classes (> 80%) for 2001-2022 (**d**) across continental Chile..

Data

Gridded meteorological and vegetation data

To derive a proxy for vegetation productivity, we used the Normalized Difference Vegetation Index (NDVI) from the MOD13A3 Collection 6.1 product derived from the MODIS (Moderate-Resolution Imaging Spectroradiometer) sensor onboard the Terra satellite.

MOD13A3 provides vegetation indices with a 1 km spatial resolution and monthly frequency[75]. For soil moisture, water supply, and water demand variables, we used ERA5-Land (ERA5L; ECMWF Reanalysis version 5 over land)[76], a reanalysis dataset that provides atmospheric and land variables since 1950. It has a spatial resolution of 0.1° (9 km), hourly frequency, and global coverage. We selected total precipitation, maximum and minimum temperature at 2 meters, and volumetric soil water layers between 0 and 100 cm of depth (layer 1 to layer 3; Supplementary Materials and Methods, Supplementary Tables 2 and 4).

Short- to long-term drought trends

Atmospheric Evaporative Demand (AED)

To compute drought indices that use water demand, it is necessary to first calculate AED. To do this, we employed the Hargreaves method[77,78] by applying the following equation:

$$AED = 0.0023 \cdot Ra \cdot (T + 17.8) \cdot \left(T_{max} - T_{min}\right)^{0.5} (1)$$

where $Ra\ \left(MJm^{2}day^{-1}\right)$ is extraterrestrial radiation; T, T_{max}, and T_{min} are mean, maximum, and minimum temperature ($°C$) at 2m. For calculating Ra we used the coordinate of the latitude of the centroid of each pixel as follows:

$$R_a = \frac{14{,}400}{\pi} \cdot G_{sc} \cdot d_r[\omega_s \cdot sin(\phi) \cdot sin(\delta) + cos(\phi) \cdot cos(\delta) \cdot sin\left(\omega_s\right)) \ (2),$$

where

Ra: extraterrestrial radiation [$MJm^{-2}day - 1$),
G_{sc}: solar constant = 0.0820 [$MJm^{-2}min^{-1}$),
d_r: inverse relative distance Earth-Sun,
ω_s sunset hour angle [rad),
ϕ: latitude [rad), and
δ: solar declination [rad).

We selected the method of Hargreaves to estimate AED because of its simplicity, as it only requires temperature and extraterrestrial radiation, and because access to the data needed for alternative methods (e.g., Penman-Monteith), which is often limited in Chile[20].

Drought indices

To derive the drought indices of water supply and demand we used the ERA5L dataset and the MODIS product (MOD13A3[79]), with a monthly frequency for 1981–2023 and 2000–2023, respectively. Drought indices capture historical anomalies of water supply and demand. To quantify each anomaly, the common practice is to derive it following a statistical parametric method in which it is assumed that the statistical distribution of the data is known[80]. The use of an erroneous statistical distribution that does not fit the data is

usually the highest source of uncertainty[81]. In the case of Chile, due to its high degree of climatic variability, it is difficult to choose a statistical distribution that can be used across its entire extent. We therefore use a non-parametric method for the calculation of the drought indices, following ref. 82.

For monitoring water supply, we used the Standardized Precipitation Index (SPI; ref. 22), which relies on precipitation data. To evaluate water demand, we chose the Evaporative Demand Drought Index (EDDI; refs. 26, 83), which is based on the AED. To consider the combined effect of water supply and demand, we selected the SPEI[17]. For SPEI, an auxiliary variable $D = P - AED$ is calculated. Soil moisture is the main driver of vegetation productivity, particularly in semi-arid regions[84]. Hence, we used the Standardized Soil Moisture Index (SSI) to monitor soil moisture (SM)[85]. For the SSI, we used the average soil moisture from ERA5L at a depth of 1m. All calculated indices are multi-scalar and can be used for the analysis of short- to long-term droughts.

To derive the drought indices, we first calculated the sum of the variables with regard to the time scale(s). In this case, for generalization purposes, we use V, referring to variables P, AED, D, and SM (Table S2). We accumulated each variable over the time series of values (months), and for the time scales s:

$$A_i^s = \sum_{i=n-s-i+2}^{n-i+1} V_i \forall i \geq n - s + 1 \quad (2)$$

The A_i^s corresponds to a moving window (convolution) that sums the variable for time scales s. This is summed over s months, starting from the most recent month (n) back in time until month n-s+1. For example, using as a variable the precipitation, a period of twelve months (n), and a time scale of three months (s):

$$A_1^3 = P_{oct} + P_{nov} + P_{dic}$$

$$\vdots = \vdots + \vdots + \vdots$$

$$A_{10}^3 = P_{jan} + P_{feb} + P_{mar}$$

Then, we used the empirical Tukey plotting position[86] over A_i^s to derive the $P\left(a_i\right)$ probabilities across a period of interest:

$$P\left(A_i^s\right) = \frac{i-0.33}{n+0.33'} \quad (3)$$

An inverse normal approximation[87] obtains the empirically derived probabilities once the variable accumulates over time for the scale s. Thus, the drought indices SPI, $SPEI$, $EDDI$, $and\ SSI$ are obtained following the

$$DI\left(A_i^s\right) = W - \frac{C_0 + C_1 \cdot W + c_2 \cdot W^2}{1 + d_1 \cdot W + d_2 \cdot W^2 + d_3 \cdot W^3} (4)$$

DI refers to the drought index calculated for the variable V. The values for the constants are: $C_0 = 2.515517$, $C_1 = 0.802853$, $C_2 = 0.010328$, $d_1 = 1.432788$, $d_2 = 0.189269$, and $d3 = 0.001308$ (Abramowitz and Stegun, 1968). For $P\left(A_i^s\right) \leq 0.5$, W=$\sqrt{-2 \cdot ln\left(P\left(A_i^s\right)\right)}$, and for $P\left(A_i^s\right) > 0.5$, replace $P\left(A_i^s\right)$ with $1 - P\left(A_i^s\right)$ and reverse the sign of $DI\left(A_i^s\right)$.

The drought indices were calculated for time scales of 1, 3, 6, 12, 24, and 36 months at a monthly frequency for 1981–2023.

Temporal trends of drought indices

To determine if there are statistically significant positive or negative temporal trends for the drought indices, we used the non-parametric modified Mann-Kendall test for serially correlated data[88]. To determine the magnitude of the trend, we used Sen's slope[89]. Sen's slope is less affected by outliers than parametric ordinary least squares (OLS) regression, and as a non-parametric method it is not influenced by the distribution of the data. We applied both methods for SPI, EDDI, SPEI, and SSI and six time scales, resulting in a total of 24 trends. We then aggregated temporal trends for each region and land cover type.

Vegetation productivity

We also used the MODIS product to calculate vegetation productivity, and calculated anomalies in NDVI using zcNDVI[34], which was derived from the monthly time series of NDVI, with Equations 2 and 4. For vegetation productivity, we selected the time scale that best correlates with annual net primary productivity (NPP) across continental Chile. For this purpose, we calculated zcNDVI for time scales of 1, 3, 6, and 12 months (from December) and compared it with the annual NPP. We obtained NPP from MOD17A3HGF[90]. We chose to use six months because the R^2 between zcNDVI and NPP reaches its highest value at six months, obtaining an R^2 of 0.31 for forest and 0.72 for shrubland (Supplementary Information Section S2). We subsequently used zcNDVI with a time scale of 6 months and calculated it at a monthly frequency for 2000–2023.

Drought impacts on vegetation productivity

For each land cover, we analyzed the trend of vegetation productivity. To this end, we identified areas within each land cover macro-class that are persistent over time, to reduce the possibility that trends in vegetation productivity may be influenced by changes in land cover. We examined the correlation between drought indices and vegetation productivity across land cover types to determine to the extent to which soil moisture and water demand and supply affect vegetation productivity.

We estimated pixel-to-pixel Pearson's correlations between drought indices at time scales of 1, 3, 6, 12, 24, and 36 months with zcNDVI. We extracted the Pearson correlation

coefficient corresponding to the time scale with the highest value. For each index, we then generated two maps: 1) a raster with values of the time scales and drought index that reached the maximum correlation, and 2) a raster with the magnitude of the correlation between the drought index and vegetation productivity.

Drought impacts on land cover change

Land cover change

To analyze land cover change, we used the classification scheme of the International Geosphere-Biosphere Programme (IGBP) from the product MCD12Q1 Collection 6.1 from MODIS. The MCD12Q1 product is produced for each year from 2001 to 2022 and defines 17 classes (see Table S1). Following the FAO classification[91], we classified native and planted forests as "forests", which represent natural and productive ecosystems dominated by large trees. To analyze the land cover change, we use the IGBP scheme from the MCD12Q1 product. We regrouped the 17 classes into ten macro-classes, as follows: 1-4 to forests (native forest and plantations), 5-7 to shrublands, 8-9 to savannas, 10 as grasslands, 11 as wetlands, 12 and 14 to croplands, 13 as urban, 15 as snow and ice, 16 as barren, and 17 as water (Table S3). This resulted in a time series of land cover with ten macro-classes for 2001 and 2023. We validated the land cover macro-classes using a high resolution (30 m) land cover map for 2013-2014[92]. Our results showed a global accuracy of ~0.82 and a F1 score of ~0.66 (Supplementary Information, S2).

We calculated the area for each land cover class in the five study regions for 2001–2022. We then estimated the temporal change in area for each land cover type and macro-class, and determined the statistical significance (p-value < 0.05) and magnitude of the trend as described above.

To assess how water demand and supply, and soil moisture affect the variation in vegetation productivity across various land cover types, we avoid analyzing areas that experienced major land cover changes in the 2001–2022 period. To assess how zcNDVI varied irrespective of land cover change, we developed a persistence mask for land cover, which only retains pixels for which the macro-class remained the same for at least 80% of the 22 years (Fig. 8d).

Relationship between land cover and drought trends

To identify which drought indices and time scales have a major impact on changes in land cover type, we examined the relationship between the trend in land cover classes and the trend in drought indices. We performed the analysis at the sub-basin scale, using 485 river basins, which have a surface area between 0.906 and 24,408 km^2 and a median area of 1,249 km^2(Supplementary Fig. S8/Table S5). For each basin, we calculated the trend per land cover type, considering the proportion of the type relative to the total surface of the basin. For each basin we extracted the average trend of all drought indices and at time scales of 1, 3, 6, 12, 24, and 36 months. Also, we extracted the average trend in zcNDVI.

We modeled trends in land cover type per macroclass with the aim of assessing how land cover trends relate to drought indices. We used the random forest method[93], which employs

multiple decision trees, allowing for classification and regression. Some advantages of random forest include the ability to find non-linear relationships, reduce overfitting, and derive variable importance. We included the four drought indices at each time scale and zcNDVI for a total of 25 predictors and built six random forest models, one for each land cover and region. We trained each model with 1000 trees using a resampling strategy with cross-validation. To this end, we used cross-validation to evaluate model fit using ten folds then calculated R^2, root mean square error (RMSE), and variable importance. Variable importance identifies which variables have a higher contribution to explaining model variation. We calculated variable importance by permuting out-of-bag (OOB) data per tree and calculating the mean standard error of the OOB data. After permuting each predictor variable, we repeated the process for the remaining variables. We repeated this process ten times per fold to assess model fit.

Finally, we visually explored the relationship between drought indices and changes in land cover. To do this, we compared the relative changes in land cover surface with the drought indices of six and thirty-six months.

Software

For downloading, processing, and analyzing spatio-temporal data, we used the R programming language for statistical computing and graphics[94]. For downloading ERA5L, we used the `{ecmwfr}` package[95]. For processing raster data, we used `{terra}`[96] and `{stars}`[97]. For managing vectorial data, we used `{sf}`[98]. For the calculation of AED, we used `{SPEI}`[99]. For mapping, we used {tmap}[100]. For data analysis and visualization, the suite {tidyverse}[101] was used. For the random forest modeling, we used the {tidymodels}[102] and {ranger}[103] packages.

Acknowledgments

The National Research and Development Agency of Chile (ANID) funded this study through the drought emergency project FSEQ210022, Fondecyt Iniciación N°11190360, Fondecyt Postdoctorado N°3230678, and Fondecyt Regular N°1210526.

References

1. Miranda, A. et al. Widespread synchronous decline of Mediterranean-type forest driven by accelerated aridity. Nature Plants 9, 1810–1817 (2023). URL https: //www.nature.com/articles/s41477-023-01541-7.
2. Calvin, K. et al. IPCC, 2023: Climate Change 2023: Synthesis Report. Contribution of Working Groups I, II and III to the Sixth Assessment Report of theIntergovernmental Panel on Climate Change [Core Writing Team, H. Lee and J. Romero (eds.)]. IPCC, Geneva, Switzerland. Tech. Rep., Intergovernmental Panel on Climate Change (IPCC) (2023). URL https://www.ipcc.ch/report/ar6/syr/.
3. Cheng, Y. et al. Scattered tree death contributes to substantial forest loss in California. Nature Communications 15, 641 (2024). URL https://www.nature.com/articles/s41467-024-44991-z.
4. Crausbay, S. D. et al. Defining Ecological Drought for the Twenty-FirstCentury. Bulletin of the American Meteorological Society 98, 2543–2550 (2017). URL https://journals.ametsoc.org/view/journals/bams/98/12/bams-d-16-0292.1.xml. Publisher: American Meteorological Society.

5. Wilhite, D. A. & Glantz, M. H. Understanding: The drought phenomenon: The role of definitions. Water International 10, 111–120 (1985). URL http: //dx.doi.org/10.1080/02508068508686328.
6. Van Loon, A. F. et al. Drought in the Anthropocene. Nature Geoscience 9, 89–91 (2016).
7. AghaKouchak, A. et al. Anthropogenic Drought: Definition, Challenges, and Opportunities. Reviews of Geophysics 59, e2019RG000683 (2021). URL https://agupubs.onlinelibrary.wiley.com/doi/10.1029/2019RG000683.
8. Lawler, J. J. et al. Projected land-use change impacts on ecosystem services in the United States. Proceedings of the National Academy of Sciences 111, 7492–7497 (2014). URL https://pnas.org/doi/full/10.1073/pnas.1405557111.
9. Newbold, T. et al. Global effects of land use on local terrestrial biodiversity. Nature 520, 45–50 (2015). URL https://www.nature.com/articles/nature14324.
10. Vicente-Serrano, S. M. et al. Global drought trends and future projections. Philosophical Transactions of the Royal Society A: Mathematical, Physical and Engineering Sciences 380, 20210285 (2022). URL https://royalsocietypublishing.org/doi/10.1098/rsta.2021.0285.
11. Kogan, F., Guo, W. & Yang, W. Near 40-year drought trend during 1981-2019 earth warming and food security. Geomatics, Natural Hazards and Risk 11, 469–490 (2020). URL https://www.tandfonline.com/doi/full/10.1080/19475705. 2020.1730452.
12. Winkler, K., Fuchs, R., Rounsevell, M. & Herold, M. Global land use changes are four times greater than previously estimated. Nature Communications 12, 2501 (2021). URL https://www.nature.com/articles/s41467-021-22702-2.
13. Song, X.-P. et al. Global land change from 1982 to 2016. Nature 560, 639–643 (2018). URL https://www.nature.com/articles/s41586-018-0411-9.
14. Chen, J. et al. Assessing the impact of drought-land cover change on global vegetation greenness and productivity. Science of The Total Environment 852, 158499 (2022). URL https://linkinghub.elsevier.com/retrieve/pii/S004896972205598X.
15. Akinyemi, F. O. Vegetation Trends, Drought Severity and Land Use-Land Cover Change during the Growing Season in Semi-Arid Contexts. Remote Sensing 2021, Vol. 13, Page 836 13, 836 (2021). URL https://www.mdpi.com/2072-4292/13/5/836/htm. Publisher: Multidisciplinary Digital Publishing Institute.
16. Peng, D. et al. Country-level net primary production distribution and response to drought and land cover change. Science of The Total Environment 574, 65–77 (2017). URL https://linkinghub.elsevier.com/retrieve/pii/S0048969716319507.
17. Vicente-Serrano, S. M., Beguería, S. & López-Moreno, J. I. A multiscalar drought index sensitive to global warming: The standardized precipitation evapotranspiration index. Journal of Climate 23, 1696–1718 (2010). URL http://dx.doi.org/10.1175/2009JCLI2909.1.
18. Craine, J. M. et al. Global diversity of drought tolerance and grassland climate-change resilience. Nature Climate Change 3, 63–67 (2013). URL https://www.nature.com/articles/nclimate1634.
19. McDowell, N. G. et al. Mechanisms of woody-plant mortality under rising drought, CO2 and vapour pressure deficit. Nature Reviews Earth & Environment 3, 294–308 (2022). URL https://www.nature.com/articles/s43017-022-00272-1.
20. Vicente-Serrano, S. M. et al. Reference evapotranspiration variability and trends in Spain, 1961–2011. Global and Planetary Change 121, 26–40 (2014). URL https://linkinghub.elsevier.com/retrieve/pii/S0921818114001180.
21. WMO, Svoboda, M., Hayes, M. & Wood, D. A. Standardized Precipitation Index User Guide (WMO, Geneva, 2012).
22. Mckee, T. B., Doesken, N. J. & Kleist, J. The relationship of drought frequency and duration to time scales. In: Proceedings of the Ninth Conference on Applied Climatology. American Metereological Society 179–184 (1993).
23. Gebrechorkos, S. H. et al. Global high-resolution drought indices for 1981–2022. Earth System Science Data 15, 5449–5466 (2023). URL https://essd.copernicus. org/articles/15/5449/2023/.
24. Liu, X., Yu, S., Yang, Z., Dong, J. & Peng, J. The first global multi-timescale daily SPEI dataset from 1982 to 2021. Scientific Data 11, 223 (2024). URL https://www.nature.com/articles/s41597-024-03047-z.
25. Vicente-Serrano, S. M., McVicar, T. R., Miralles, D. G., Yang, Y. & Tomas-Burguera, M. Unraveling the influence of atmospheric evaporative demand on drought and its response to climate change. WIREs Climate Change 11, e632 (2020). URL https://wires.onlinelibrary.wiley.com/doi/10.1002/wcc.632.
26. McEvoy, D. J. et al. The Evaporative Demand Drought Index. Part II: CONUS-Wide Assessment against Common Drought Indicators. Journal of Hydrometeorology 17, 1763–1779 (2016). URL http://journals.ametsoc.org/doi/10.1175/JHM-D-15-0122.1.
27. Narasimhan, B. & Srinivasan, R. Development and evaluation of Soil Moisture Deficit Index (SMDI) and Evapotranspiration Deficit Index (ETDI) for agricultural drought monitoring. Agricultural and Forest Meteorology 133, 69–88 (2005). URL https://linkinghub.elsevier.com/retrieve/pii/S0168192305001565.
28. Souza, A. G. S. S., Ribeiro Neto, A. & Souza, L. L. D. Soil moisture-based index for agricultural drought assessment: SMADI application in Pernambuco State-Brazil. Remote Sensing of Environment 252, 112124 (2021). URL https://linkinghub.elsevier.com/retrieve/pii/S0034425720304971.
29. AghaKouchak, A. A baseline probabilistic drought forecasting framework using standardized soil moisture index: application to the 2012 United States drought. Hydrology and Earth System Sciences 18, 2485–2492 (2014). URL https://hess.copernicus.org/articles/18/2485/2014/.

30. AghaKouchak, A. et al. Remote sensing of drought: Progress, challenges and opportunities. Reviews of Geophysics 53, 452–480 (2015). URL http://dx.doi. org/10.1002/2014RG000456.
31. Camps-Valls, G. et al. A unified vegetation index for quantifying the terrestrial biosphere. Science Advances 7, eabc7447 (2021). URL https://www.science.org/doi/10.1126/sciadv.abc7447.
32. Paruelo, J. M. et al. An integrative index of Ecosystem Services provision based on remotely sensed data. Ecological Indicators 71, 145–154 (2016). URL https://www.sciencedirect.com/science/article/pii/S1470160X16303843. Publisher:Elsevier.
33. Helman, D., Mussery, A., Lensky, I. M. & Leu, S. Detecting changes in biomass productivity in a different land management regimes in drylands using satellite-derived vegetation index. Soil Use and Management 30, 32–39 (2014). URL https://bsssjournals.onlinelibrary.wiley.com/doi/10.1111/sum.12099.
34. Zambrano, F., Vrieling, A., Nelson, A., Meroni, M. & Tadesse, T. Prediction of drought-induced reduction of agricultural productivity in Chile from MODIS, rainfall estimates, and climate oscillation indices. Remote Sensing of Environment 219, 15–30 (2018). URL https://www.sciencedirect.com/science/article/pii/S0034425718304541. Publisher: Elsevier.
35. Beck, H. E. et al. High-resolution (1 km) Köppen-Geiger maps for 1901–2099 based on constrained CMIP6 projections. Scientific Data 10 (2023). URL http://dx.doi.org/10.1038/s41597-023-02549-6.
36. Luebert, F. & Pliscoff, P. The vegetation of Chile and the EcoVeg approach in the context of the International Vegetation Classification project. Vegetation Classification and Survey 3, 15–28 (2022). URL https://vcs.pensoft.net/article/67893/.
37. Garreaud, R. et al. The 2010-2015 mega drought in Central Chile: Impacts on regional hydroclimate and vegetation. Hydrology and Earth System Sciences Discussions 2017, 1–37 (2017). URL http://www.hydrol-earth-syst-sci-discuss.net/hess-2017-191/.
38. Miranda, A. et al. Forest browning trends in response to drought in a highly threatened mediterranean landscape of South America. Ecological Indicators 115, 106401 (2020). URL https://linkinghub.elsevier.com/retrieve/pii/S1470160X20303381.
39. Urrutia-Jalabert, R., González, M. E., González-Reyes, ., Lara, A. & Garreaud, R. Climate variability and forest fires in central and south-central Chile. Ecosphere 9, e02171 (2018). URL https://esajournals.onlinelibrary.wiley.com/doi/10.1002/ecs2.2171.
40. Venegas-González, A., Juñent, F. R., Gutiérrez, A. G. & Filho, M. T. Recent radial growth decline in response to increased drought conditions in the northernmost Nothofagus populations from South America. Forest Ecology and Management 409, 94–104 (2018). URL https://linkinghub.elsevier.com/retrieve/pii/S0378112717313993.
41. Zambrano, F., Lillo-Saavedra, M., Verbist, K. & Lagos, O. Sixteen years of agricultural drought assessment of the biobío region in chile using a 250 m resolution vegetation condition index (VCI). Remote Sensing 8, 1–20 (2016). URL http://www.mdpi.com/2072-4292/8/6/530. Publisher: Multidisciplinary Digital Publishing Institute.
42. Zambrano, F. in Four decades of satellite data for agricultural drought monitoring throughout the growing season in Central Chile (eds Vijay P. Singh Deepak Jhajharia, R. M. & Kumar, R.) Integrated Drought Management, Two Volume Set 28 (CRC Press, 2023).
43. Zúñiga, F., Jaime, M. & Salazar, C. Crop farming adaptation to droughts in small-scale dryland agriculture in Chile. Water Resources and Economics 34, 100176 (2021). URL https://linkinghub.elsevier.com/retrieve/pii/S2212428421000013.
44. Boisier, J. P. et al. Anthropogenic drying in central-southern Chile evidenced by long-term observations and climate model simulations. Elementa 6, 74 (2018). URL https://www.elementascience.org/article/10.1525/elementa.328/.
45. Sarricolea, P., Meseguer-Ruiz, ., Serrano-Notivoli, R., Soto, M. V. & Martin-Vide, J. Trends of daily precipitation concentration in Central-Southern Chile. Atmospheric Research 215, 85–98 (2019). URL https://linkinghub.elsevier.com/retrieve/pii/S0169809518308512.
46. Rashid, M. M. & Beecham, S. Characterization of meteorological droughts across South Australia. Meteorological Applications 26, 556–568 (2019). URL https://rmets.onlinelibrary.wiley.com/doi/10.1002/met.1783.
47. Miró, J. J., Estrela, M. J., Corell, D., Gómez, I. & Luna, M. Y. Precipitation and drought trends (1952–2021) in a key hydrological recharge area of the eastern Iberian Peninsula. Atmospheric Research 286, 106695 (2023). URL https://linkinghub.elsevier.com/retrieve/pii/S0169809523000923.
48. Páscoa, P. et al. A high-resolution view of the recent drought trends over the Iberian Peninsula. Weather and Climate Extremes 32, 100320 (2021). URL https://linkinghub.elsevier.com/retrieve/pii/S2212094721000189.
49. Taucare, M., Viguier, B., Figueroa, R. & Daniele, L. The alarming state of Central Chile's groundwater resources: A paradigmatic case of a lasting over-exploitation. Science of The Total Environment 906, 167723 (2024). URL https://linkinghub.elsevier.com/retrieve/pii/S0048969723063507.
50. Nicolai-Shaw, N., Zscheischler, J., Hirschi, M., Gudmundsson, L. & Seneviratne, I. A drought event composite analysis using satellite remote-sensing based soil moisture. Remote Sensing of Environment 203, 216–225 (2017). URL https://linkinghub.elsevier.com/retrieve/pii/S0034425717302729.
51. Jiang, W., Wang, L., Feng, L., Zhang, M. & Yao, R. Drought characteristics and its impact on changes in surface vegetation from 1981 to 2015 in the Yangtze River Basin, China. International Journal of Climatology 40, 3380–3397 (2020). URL https://rmets.onlinelibrary.wiley.com/doi/10.1002/joc.6403.

52. Zhou, K., Li, J., Zhang, T. & Kang, A. The use of combined soil moisture data to characterize agricultural drought conditions and the relationship among different drought types in China. Agricultural Water Management 243, 106479 (2021). URL https://linkinghub.elsevier.com/retrieve/pii/S0378377420305965.
53. Bonan, G. B. Forests and Climate Change: Forcings, Feedbacks, and the Climate Benefits of Forests. Science 320, 1444–1449 (2008). URL https://www.science. org/doi/10.1126/science.1155121.
54. Venegas-González, A. et al. Sclerophyllous Forest Tree Growth Under the Influence of a Historic Megadrought in the Mediterranean Ecoregion of Chile. Ecosystems 26, 344–361 (2023). URL https://link.springer.com/10.1007/s10021-022-00760-x.
55. Oliveira, R. S. et al. Deep root function in soil water dynamics in cerrado savannas of central Brazil. Functional Ecology 19, 574–581 (2005). URL https://besjournals.onlinelibrary.wiley.com/doi/10.1111/j.1365-2435.2005.01003.x.
56. Holden, Z. A. et al. Decreasing fire season precipitation increased recent western US forest wildfire activity. Proceedings of the National Academy of Sciences 115 (2018). URL https://pnas.org/doi/full/10.1073/pnas.1802316115.
57. González, M. E., Gómez-González, S., Lara, A., Garreaud, R. &Díaz-Hormazábal, I. The 2010–2015 Megadrought and its influence on the fireregime in central and south-central Chile. Ecosphere 9, e02300 (2018). URLhttps://esajournals.onlinelibrary.wiley.com/doi/10.1002/ecs2.2300.
58. Bowman, D. M. J. S. et al. Human–environmental drivers and impacts of the globally extreme 2017 Chilean fires. Ambio 48, 350–362 (2019). URL http://link.springer.com/10.1007/s13280-018-1084-1.
59. Quiring, S. M. & Ganesh, S. Evaluating the utility of the Vegetation Condition Index (VCI) for monitoring meteorological drought in Texas. Agricultural and Forest Meteorology 150, 330–339 (2010). URL http://www.sciencedirect.com/science/article/pii/S0168192309002809.
60. Muñoz, A. A. et al. Water Crisis in Petorca Basin, Chile: The Combined Effects of a Mega-Drought and Water Management. Water 12, 648 (2020). URL https://www.mdpi.com/2073-4441/12/3/648.
61. Duran-Llacer, I. et al. Lessons to Be Learned: Groundwater Depletion in Chile's Ligua and Petorca Watersheds through an Interdisciplinary Approach. Water 12, 2446 (2020). URL https://www.mdpi.com/2073-4441/12/9/2446.
62. Carrasco, G. et al. Effects of climate change on forest plantation productivity in Chile. Global Change Biology 28, 7391–7409 (2022). URL https://onlinelibrary.wiley.com/doi/10.1111/gcb.16418.
63. Fajardo, A., Gazol, A., Mayr, C. & Camarero, J. J. Recent decadal drought reverts warming-triggered growth enhancement in contrasting climates in the southern Andes tree line. Journal of Biogeography 46, 1367–1379 (2019). URLhttps://onlinelibrary.wiley.com/doi/10.1111/jbi.13580.
64. Holz, A., Hart, S. J., Williamson, G. J., Veblen, T. T. & Aravena, J. C. Radial growth response to climate change along the latitudinal range of the world's southernmost conifer in southern South America. Journal of Biogeography 45, 1140–1152 (2018). URL https://onlinelibrary.wiley.com/doi/10.1111/jbi.13199.
65. Segovia, R. A. et al. Freezing and water availability structure the evolutionary diversity of trees across the Americas. Science Advances 6, eaaz5373 (2020). URL https://www.science.org/doi/10.1126/sciadv.aaz5373.
66. Sabatini, F. M. et al. Global patterns of vascular plant alpha diversity. Nature Communications 13, 4683 (2022). URL https://www.nature.com/articles/s41467-022-32063-z.
67. Brêda, J. P. L. F. et al. Climate change impacts on South American water balance from a continental-scale hydrological model driven by CMIP5 projections. Climatic Change 159, 503–522 (2020). URL http://link.springer.com/10.1007/s10584-020-02667-9.
68. Scheffer, M., Carpenter, S., Foley, J. A., Folke, C. & Walker, B. Catastrophic shifts in ecosystems. Nature 413, 591–596 (2001). URL https://www.nature.com/articles/35098000.
69. Martínez-Vilalta, J. & Lloret, F. Drought-induced vegetation shifts in terrestrial ecosystems: The key role of regeneration dynamics. Global and Planetary Change 144, 94–108 (2016). URL https://linkinghub.elsevier.com/retrieve/pii/S0921818115301405.
70. Hermans, K. & McLeman, R. Climate change, drought, land degradation and migration: exploring the linkages. Current Opinion in Environmental Sustainability 50, 236–244 (2021). URL https://linkinghub.elsevier.com/retrieve/pii/S1877343521000701.
71. Eldridge, D. J.et al.Impacts of shrub encroachment on ecosystem structureand functioning: towards a global synthesis: Synthesizing shrub encroachment effects. Ecology Letters 14, 709–722 (2011). URLhttps://onlinelibrary.wiley.com/doi/10.1111/j.1461-0248.2011.01630.x.
72. Götmark, F., Götmark, E. & Jensen, A. M. Why Be a Shrub? A Basic Model and Hypotheses for the Adaptive Values of a Common Growth Form. Frontiers in Plant Science 7 (2016). URL http://journal.frontiersin.org/Article/10.3389/fpls.2016.01095/abstract.
73. Aceituno, P., Boisier, J. P., Garreaud, R., Rondanelli, R. & Rutllant, J. A. in Climate and Weather in Chile (eds Fernández, B. & Gironás, J.) Water Resources of Chile, Vol. 8 7–29 (Springer International Publishing, Cham, 2021).
74. Garreaud, R. D. The Andes climate and weather. Advances in Geosciences 22, 3–11 (2009). URL https://adgeo.copernicus.org/articles/22/3/2009/.

75. Didan, K. MOD13Q1 MODIS/Terra Vegetation Indices 16-Day L3 Global 250m SIN Grid V006. Tech. Rep., NASA EOSDIS Land Processes DAAC (2015).
76. Muñoz-Sabater, J. et al. ERA5-Land: a state-of-the-art global reanalysis dataset for land applications. Earth System Science Data 13, 4349–4383 (2021). URL https://essd.copernicus.org/articles/13/4349/2021/.
77. Hargreaves, G. H. Defining and Using Reference Evapotranspiration. Journal of Irrigation and Drainage Engineering 120, 1132–1139 (1994). URL https://ascelibrary.org/doi/10.1061/%28ASCE%290733-9437%281994%29120%3A6%281132%29.
78. Hargreaves, G. H. & Samani, Z. A. Reference crop evapotranspiration from temperature. Applied engineering in agriculture 1, 96–99 (1985).
79. Didan, K. MOD13A3 MODIS/Terra Vegetation Indices Monthly L3 Global 1kmSIN Grid V006 (2015). URL https://lpdaac.usgs.gov/products/mod13a3v006/.
80. Heim, R. R. A Review of Twentieth-Century Drought Indices Used in the United States. Bulletin of the American Meteorological Society 83, 1149–1166 (2002). URL https://journals.ametsoc.org/doi/10.1175/1520-0477-83.8.1149.
81. Laimighofer, J. & Laaha, G. How standard are standardized drought indices? Uncertainty components for the SPI & SPEI case. Journal of Hydrology 613, 128385 (2022). URL https://linkinghub.elsevier.com/retrieve/pii/S0022169422009544.
82. Farahmand, A. & AghaKouchak, A. A generalized framework for deriving nonparametric standardized drought indicators. Advances in Water Resources 76, 140–145 (2015). URL https://linkinghub.elsevier.com/retrieve/pii/S0309170814002322.
83. Hobbins, M. T. et al. The Evaporative Demand Drought Index. Part I: Linking Drought Evolution to Variations in Evaporative Demand. Journal of Hydrometeorology 17, 1745–1761 (2016). URL http://journals.ametsoc.org/doi/10.1175/JHM-D-15-0121.1.
84. Li, W. et al. Widespread increasing vegetation sensitivity to soil moisture. Nature Communications 13, 3959 (2022). URL https://www.nature.com/articles/s41467-022-31667-9.
85. Hao, Z. & AghaKouchak, A. Multivariate Standardized Drought Index: A parametric multi-index model. Advances in Water Resources 57, 12–18 (2013). URL https://linkinghub.elsevier.com/retrieve/pii/S0309170813000493.
86. Wilks, D. S. Empirical distributions and exploratory data analysis. Statistical Methods in the Atmospheric Sciences 100 (2011).
87. Abramowitz, M. & Stegun, I. A. Handbook of mathematical functions with formulas, graphs, and mathematical tables Vol. 55 (US Government printing office, 1968).
88. Yue, S. & Wang, C. The Mann-Kendall Test Modified by Effective Sample Size to Detect Trend in Serially Correlated Hydrological Series. Water Resources Management 18, 201–218 (2004). URL http://link.springer.com/10.1023/B:WARM.0000043140.61082.60.
89. Sen, P. K. Estimates of the Regression Coefficient Based on Kendall's Tau. Journal of the American Statistical Association 63, 1379–1389 (1968). URL http://www.tandfonline.com/doi/abs/10.1080/01621459.1968.10480934.
90. Running, S. & Zhao, M. MOD17A3HGF MODIS/Terra Net Primary Production Gap-Filled Yearly L4 Global 500 m SIN Grid V006 (2019). URL https://lpdaac.usgs.gov/products/mod17a3hgfv006/.
91. FAO. The State of the World's Forests 2022 (FAO, 2022). URL http://www.fao.org/documents/card/en/c/cb9360en.
92. Zhao, Y. et al. Detailed dynamic land cover mapping of Chile: Accuracy improvement by integrating multi-temporal data. Remote Sensing of Environment 183, 170–185 (2016). URL https://linkinghub.elsevier.com/retrieve/pii/S0034425716302188.
93. Ho, T. K. Random decision forests, Vol. 1, 278–282 (IEEE, 1995).
94. R Core Team. R: A Language and Environment for Statistical Computing (R Foundation for Statistical Computing, Vienna, Austria, 2023). URL https://www.R-project.org/.
95. Hufkens, K., Stauffer, R. & Campitelli, E. The ecwmfr package: an interface to ECMWF API endpoints (2019). URL https://bluegreen-labs.github.io/ecmwfr/.
96. Hijmans, R. J. terra: Spatial Data Analysis (2023). URL https://CRAN.R-project.org/package=terra.
97. Pebesma, E. & Bivand, R. Spatial Data Science: With applications in R (Chapman and Hall/CRC, London, 2023). URL https://r-spatial.org/book/.
98. Pebesma, E. Simple Features for R: Standardized Support for Spatial Vector Data. The R Journal 10, 439–446 (2018). URL https://doi.org/10.32614/RJ-2018-009.
99. Beguería, S. & Vicente-Serrano, S. M. SPEI: Calculation of the Standardized Precipitation-Evapotranspiration Index (2023). URL https://CRAN.R-project.org/package=SPEI.
100. Tennekes, M. tmap: Thematic Maps in R. Journal of Statistical Software 84, 1–39 (2018).
101. Wickham, H. et al. Welcome to the tidyverse. Journal of Open Source Software 4, 1686 (2019).
102. Kuhn, M. & Wickham, H. Tidymodels: a collection of packages for modeling and machine learning using tidyverse principles. (2020). URL https://www.tidymodels.org.
103. Wright, M. N. & Ziegler, A. ranger: A Fast Implementation of Random Forests for High Dimensional Data in C++ and R. Journal of Statistical Software 77,1–17 (2017).